

# Preparation and characterization of poly (vinylidene fluoride)/TiO<sub>2</sub> hybrid membranes

Weiyang LI (✉)<sup>1</sup>, Xiuli SUN<sup>2</sup>, Chen WEN<sup>3</sup>, Hui LU<sup>2</sup>, Zhiwei WANG<sup>1</sup>

<sup>1</sup> State Key Laboratory of Pollution Control and Resource Reuse, School of Environmental Science and Engineering, Tongji University, Shanghai 200092, China

<sup>2</sup> Key Laboratory of Yangtze Water Environment of Ministry of Education, School of Environmental Science and Engineering, Tongji University, Shanghai 200092, China

<sup>3</sup> School of Environmental and Chemical Engineering, Tianjin Polytechnic University, Tianjin 300160, China

© Higher Education Press and Springer-Verlag Berlin Heidelberg 2012

**Abstract** Poly(vinylidene fluoride) (PVDF)/titanium dioxide (TiO<sub>2</sub>) hybrid membranes were prepared using nano-TiO<sub>2</sub> as the modifier, and characterized by Transmission Electron Microscope (TEM), Fourier transform infrared spectroscopy (FT-IR), scanning electron microscope (SEM), atomic force microscope (AFM), X-ray diffraction (XRD) and X-ray photoelectron spectroscopy (XPS). The characterization results demonstrated that nano-sized TiO<sub>2</sub> particles dispersed homogeneously within the PVDF matrix, contributing to more hydroxyls and smoother surfaces. Moreover, permeate flux, retention factor, porosity, contact angle and anti-fouling tests were carried out to evaluate the effect of TiO<sub>2</sub> concentration on the performance of PVDF membranes. Among all the prepared membranes, PVDF/TiO<sub>2</sub> membrane containing 10 vol.% TiO<sub>2</sub> exhibited the best hydrophilicity with an average pure water flux up to 237 L·m<sup>-2</sup>·h<sup>-1</sup>, higher than that of unmodified PVDF membranes (155 L·m<sup>-2</sup>·h<sup>-1</sup>). Besides, the bovine serum albumin rejection of the hybrid membrane was improved evidently from 52.3% to 70.6%, and the contact angle was significantly lowered from 83° to 60°, while the average pore size and its distribution became smaller and narrower.

**Keywords** poly(vinylidene fluoride) (PVDF) membrane, nano-TiO<sub>2</sub>, anti-fouling performance, water treatment

## 1 Introduction

Poly(vinylidene fluoride) (PVDF) is a frequently used material in the manufacturing of ultrafiltration (UF), microfiltration (MF), and pervaporation (PV) membranes due to its competent properties, such as excellent thermal and chemical stability, radiation resistance, etc [1,2]. Many investigations have been done on the PVDF membranes. Some researchers focused on their application in water treatment [3,4], and the others concentrated on the membrane formation mechanism [5]. However, the strong fouling propensity of PVDF membranes poses challenges, especially the significant nonspecific adsorption of organics due to the intrinsic low surface energy and hydrophobicity of PVDF polymer [6–8].

It is widely accepted that the anti-fouling characteristics of hydrophilic membranes are better than those of hydrophobic ones. As a result, modification of PVDF membranes to increase their hydrophilicity is very important [9]. Typically, three methods can be used to hydrophilize PVDF MF membrane: 1) mixing hydrophilic polymer with PVDF to form functionalized membranes, 2) grafting hydrophilic branches to hydrophobic PVDF backbone, and 3) coating a hydrophilic layer on the PVDF membrane surface. Among these processes, the methods of modifying the membrane surface include UV irradiation, plasma treatment, gamma irradiation, chemical grafting, and so on [10–12]. The addition of inorganic fillers, especially the nanoparticles, has led to increased membrane permeability and improved control of membrane properties [13]. Nanoparticles have unique electronic, magnetic and optical properties to improve the capabilities of polymers to a certain extent because of their small sizes, large specific surface areas and strong activities [14,15]. To date, many kinds of inorganic

nanoparticles, such as SiO<sub>2</sub>, Al<sub>2</sub>O<sub>3</sub>, Fe<sub>3</sub>O<sub>4</sub>, ZnO, ZrO<sub>2</sub>, CdS and TiO<sub>2</sub>, have been used in membrane preparation [16–19]. Among these inorganic nanoparticles, titanium dioxide (TiO<sub>2</sub>) is quite popular for its innocuity, resisting and decomposing bacteria, UV-proof and super hydrophilicity [20]. Many polymer/TiO<sub>2</sub> nanocomposite membranes were prepared by simply incorporating TiO<sub>2</sub> nanoparticles into the polymer matrix [21–23], but there is still much to be done. Although it is facile to blend or coat PVDF with the commercial TiO<sub>2</sub>, new problems occurred, such as particle agglomeration and poor compatibility between the nanoparticles and the matrix [24].

The main purpose of this study is to enhance the compatibility between the nanoparticles and the membrane matrix, and to improve the overall performance of PVDF membranes. In the present study, nano-TiO<sub>2</sub> was prepared through the hydrolysis of tetrabutyl titanate. Different PVDF/TiO<sub>2</sub> hybrid membranes were prepared with nano-TiO<sub>2</sub> as the modifier. Performances of the membranes were investigated by the pure water filtration and anti-fouling tests. Several analytical techniques, including Fourier transform infrared spectroscopy (FT-IR), scanning electron microscope (SEM), atomic force microscope (AFM), X-ray diffraction (XRD) and X-ray photoelectron spectroscopy (XPS) were applied to analyze the structural properties. The mechanical strength of PVDF membrane was also studied.

## 2 Materials and methods

### 2.1 Materials

PVDF powder (commercial purity) was purchased from Shanghai 3F New Materials Co., Ltd, China. *N,N*-dimethylacetamide (DMAc) (analytical purity), polyvinylpyrrolidone (PVP) (analytical purity) and tetrabutyl titanate (chemical purity) were purchased from Tianjin Chemical Reagent Factory, China. Nitric acid (chemical purity) was purchased from Beijing Chemical Plant, China. Bovine serum albumin (BSA) (chemical purity) was purchased from Shanghai Lanji Science and Technology Co., Ltd, China.

### 2.2 Modification of PVDF membranes

Before PVDF membrane was modified, nano-TiO<sub>2</sub> was prepared first in the following procedure: 0.1 g PVP was added to 100.0 mL DMAc (solution A). Under continuous stirring, 10.0 mL tetrabutyltitanate was dropped slowly to solution B, which consisted of 10.0 mL liquid from solution A, 2.0 mL deionized water and 1.0 mL nitric acid. After the mixture got milky white, another 10.0 mL of solution A was added dropwise to it. Then the new mixed solution was placed in a water bath at 75°C with

vigorous stirring for 8 h. After mixing uniformly, stable and yellow transparent nano-TiO<sub>2</sub> was obtained.

Nano-TiO<sub>2</sub> obtained above with different contents (0 vol.%, 5 vol.%, 10 vol.% and 12 vol.%) was added dropwise to the casting solution, which contains 18 wt.% PVDF, 7 wt.% additive PVP and 75 wt.% DMAc. The above mixture solution was stirred for 24 h at 65°C constantly, and then was degassed for 48 h to remove air bubbles. Subsequently, the mixed polymer solution was cast on a glass plate at room temperature. The thickness of the wet membranes was kept at about 0.2 mm. After exposure in air for 10 s, the glass plate with casting solution was immediately immersed into a water bath for 1–2 days to remove the remaining solvent. Then the nascent membrane was stored in demineralized water containing 1% formaldehyde to inhibit bacteria growth.

These membranes prepared above are designated as PVDF/TiO<sub>2</sub>-X, where X is the volume ratio of nano-TiO<sub>2</sub> in the membrane casting solution. The membrane was just designated as PVDF when X equaled 0.

### 2.3 Characterization of the membrane surfaces

5 mL prepared TiO<sub>2</sub> sol was dried in the air in order to get the TiO<sub>2</sub> powder, which was then examined by a transmission electron microscope (TEM) (TECNAI G2F20, Philips, Netherlands).

The XRD patterns of the membrane samples were obtained using a diffractometer (Bruker D8, Germany) with monochromatized Cu K $\alpha$  characteristic radiation (wavelength = 0.154 nm, at 40 kV, 40 mA, in a 2 $\theta$  range of 5°–80°) at room temperature.

The membrane surface morphology was observed using an AFM (AFM/STM5500, Agilent, USA) at room temperature. After image acquisition, root mean square (RMS) roughness of the membrane surface was determined by a program in the AFM image processing toolbox. The membranes were air-dried before AFM observation.

The surface and cross-sectional morphologies of the membranes were examined by an SEM (TECNAI G2F20, Philips, Netherlands). The samples were sprayed with a thin gold layer before SEM observation.

The surface chemical structure and composition of the membranes were investigated using an FT-IR spectroscope (TENSOR 37, Bruker, Germany).

Clean and fouled PVDF membranes were characterized by an XPS (K-Alpha, Thermo Scientific, USA). The fouled membranes were taken from the permeation cell after the filtration of BSA for 2.5 h, and then rinsed with pure water for 30 min before analysis.

### 2.4 Filtration and antifouling tests

The pure water flux of the membranes was measured using a cross-flow filtration cell. A membrane of 21.23 cm<sup>2</sup> in effective area was first compacted for 30 min at 0.1 MPa.

Then the pure water flux was measured at 0.1 MPa till the flux reached a steady-state. The pure water flux was calculated by the following equation:

$$J = V/(A \cdot t), \quad (1)$$

where  $J$  is the pure water flux ( $\text{L} \cdot \text{m}^{-2} \cdot \text{h}^{-1}$ ),  $V$  is the permeate volume (L),  $A$  is the membrane area ( $\text{m}^2$ ) and  $t$  is the time (h). Each type of membranes was repeatedly tested for five times and the average value was reported.

The BSA rejection experiments were carried out with  $0.8 \text{ g} \cdot \text{L}^{-1}$  BSA aqueous solution at the pressure of 0.1 MPa. The protein concentration was determined using a UV-Vis spectrophotometer at the wavelength of 280 nm (UV-Vis 2450, Shimadzu, Japan). The BSA rejection ( $R$ ) was calculated by Eq. (2).

$$R = \frac{C_0 - C_p}{C_0} \times 100\%, \quad (2)$$

where  $C_p$  ( $\text{mg} \cdot \text{L}^{-1}$ ) and  $C_0$  ( $\text{mg} \cdot \text{L}^{-1}$ ) are the solute concentrations of permeate and feed solutions, respectively.

The porosity was measured by a mercury porosimeter (Demo AutoPore IV 9510, Micromeritics, USA). The micropores of the membranes were filled with mercury first, and then the volumes of the mercury filled under different pressures were measured.

The anti-fouling performance of the membranes was evaluated by the cross-flow filtration system (Fig. 1).  $0.8 \text{ g} \cdot \text{L}^{-1}$  BSA aqueous solution was used as the feed. The variation of permeate flux with time was recorded. And the normalized permeate flux ( $R_p$ ) was calculated by Eq. (3).

$$R_p = \frac{J_1}{J} \times 100\%, \quad (3)$$

where  $J_1$  and  $J$  are the permeate flux of BSA aqueous solution and pure water flux for the corresponding membranes, respectively.

Pore size distribution was measured with a PMI Bubble

Point Tester pore size distribution analyzer (Porous Materials Co., Ltd., USA).

The contact angle between water and membrane surface was measured to evaluate the membrane hydrophilicity, using a JYSP-180 contact angle goniometer (Jinshengxin Inspection Instrument Co., Ltd, Beijing, China). The contact angles were measured nine times for each sample and then were averaged to minimize the experimental error.

## 2.5 Mechanical stability

Tensile strength and elongation of the prepared membranes were measured by a material testing machine (YG(B) 026H-500, Darong Machines Ltd., Zhejiang, China) at a loading velocity of 50 mm/min. The average width and thickness of the membranes were 50 and 0.2 mm, respectively. The reported results were the average value of at least five samples.

## 3 Results and discussion

### 3.1 Separation performance

Figure 2 shows the TEM images of the  $\text{TiO}_2$  powder, from which we can see that the basic  $\text{TiO}_2$  particles are round and the average particle size is about  $(6.1 \pm 2) \text{ nm}$ .

The influences of  $\text{TiO}_2$  contents on pure water flux are shown in Table 1. It could be observed that the water flux reached a peak value at the 10 vol.% loading, which was 52.7% higher than that of pure PVDF membranes. This could partially be ascribed to an increment in porosity (Table 2) (to minimize the experiment error, each sample were determined more than 5 times, and the Standard Deviations (SD) were as low as 0.4%). However, the increasing degree of the porosity was not very high, and the pore size of the hybrid membranes actually decreased as illustrated in Fig. 3. And it was also reported that the

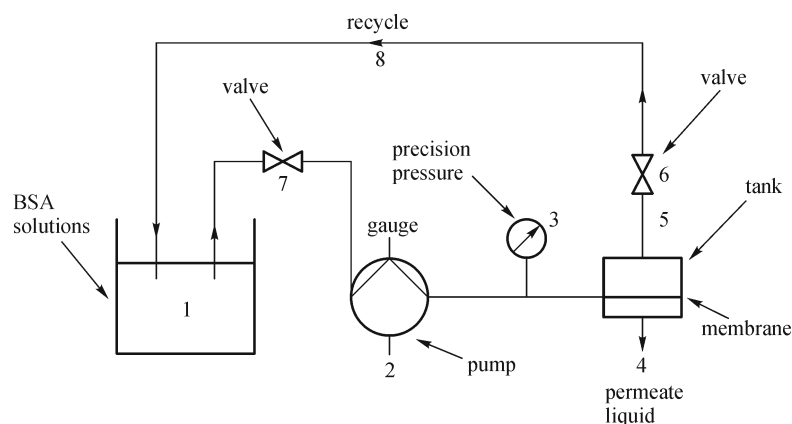
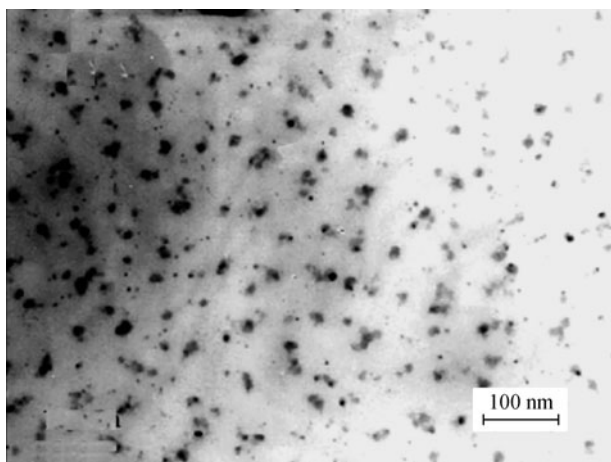


Fig. 1 The membrane evaluation device

**Table 1** The performance of the membranes

samples	pure water flux /( $L \cdot m^{-2} \cdot h^{-1}$ )	contact angle/(°)	retention to BSA/%
PVDF	155	82.8	52.3
PVDF/TiO <sub>2</sub> -5%	203	65.9	62.6
PVDF/TiO <sub>2</sub> -10%	237	59.7	70.6
PVDF/TiO <sub>2</sub> -12%	206	61.6	60.8

**Fig. 2** TEM micrograph of TiO<sub>2</sub> particles

decrease of pore size usually deteriorates the permeability [25]. Therefore, the rapid enhancement of permeate flux might be mainly attributed to TiO<sub>2</sub> which preferentially facilitated the transport of more water molecules [26]. However, when the TiO<sub>2</sub> loading was greater than 10 vol.%, the permeate flux of PVDF/TiO<sub>2</sub> hybrid membranes decreased. It might be due to the fact that high nano-TiO<sub>2</sub> concentration produced highly viscous casting solution (Table 2), which slowed down the formation process of hybrid membranes, causing to form a thicker skinlayer and a compact network sublayer that contains considerable TiO<sub>2</sub> particles which could block membrane pores. Therefore, it could exert a negative effect on permeability.

Rejection of the membranes can reflect their separation characteristics, and usually a higher rejection indicates a better separation performance. It should be noted that the rejection of the modified membrane with 0.8 g·L<sup>-1</sup> BSA solution was remarkably higher than that of the unmodified membrane (Table 1). In particular, the rejection of

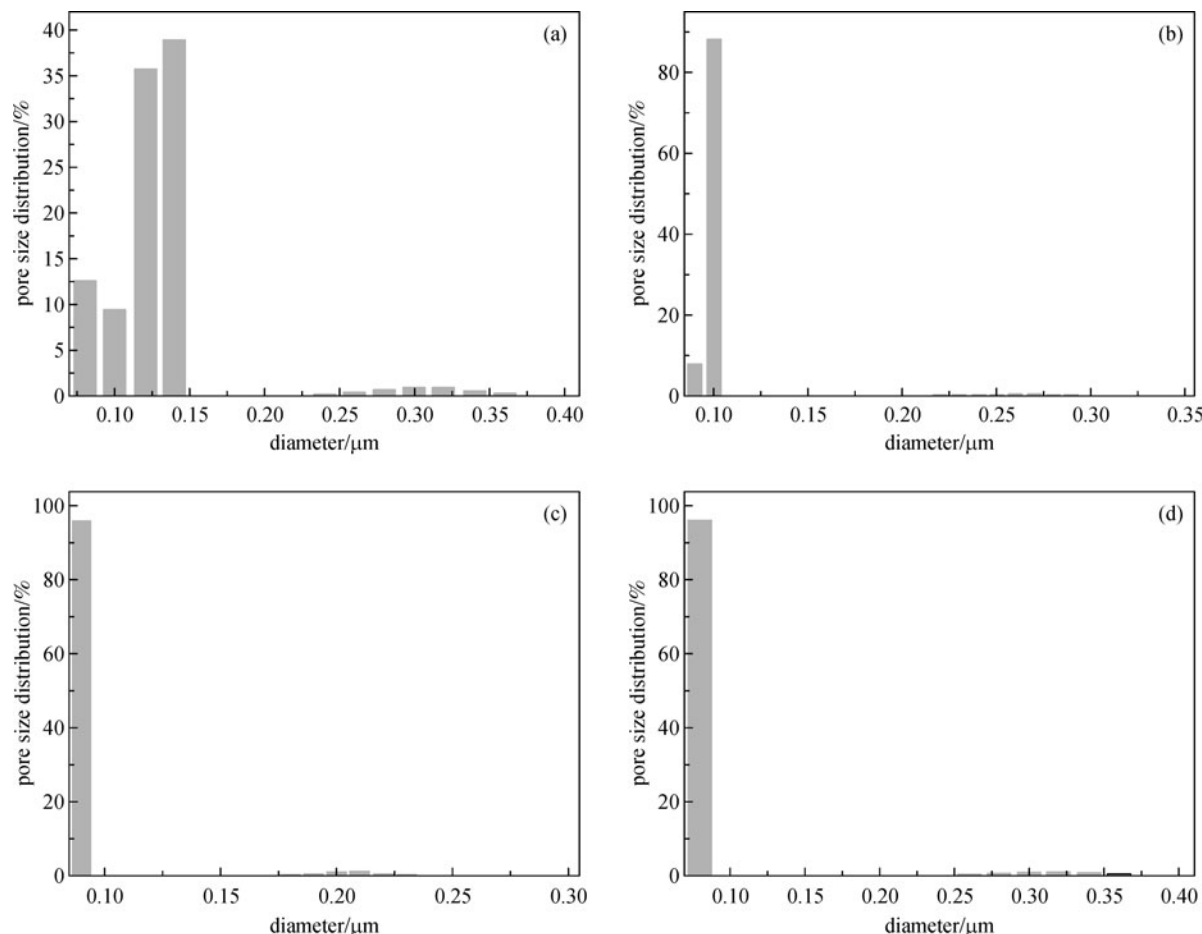
PVDF/TiO<sub>2</sub>-10% membrane reached 70.6%, which was increased by almost 35% compared to the initial one. It demonstrated that the separation performance of the hybrid membrane was enhanced greatly. That is because the size of nano-TiO<sub>2</sub> particles was so small that it was easy for them to disperse uniformly in the matrix to regulate the microstructure, and it is also owing to the balance between porosity increase and compact structure of organic-inorganic network, thus the rejection is greatly improved.

Figure 3 illustrates the pore size distribution of the prepared membranes. The most pores of the PVDF membrane were found between 0.05 and 0.38 μm, while pores of the hybrid membranes were around 0.08 μm. It showed that the addition of different amounts of TiO<sub>2</sub> changed the pore size distribution of membranes. The number of small pores increased with increasing the nano-TiO<sub>2</sub> loading. The PVDF membrane showed the widest pore size distribution, whereas the PVDF/TiO<sub>2</sub>-10% membrane showed the narrowest pore size distribution. This could be explained as follows: the nano-TiO<sub>2</sub> at a proper content could greatly enhance the mass transfer resistance between solvent and nonsolvent, and then eliminate the stress within or between the molecules, so that the compact pore structure was formed and finally the pore size distribution was narrowed.

To investigate the anti-fouling performance of the prepared membranes, protein (BSA) solution filtration experiments were conducted, and typical results are shown in Fig. 4. It is observed that the PVDF/TiO<sub>2</sub>-10% exhibits a relatively smooth change in normalized permeate flux, while that of the pure PVDF membrane dropped dramatically. The fouling was primarily originated from the gel layer formation. The strong hydrophilicity of the nano-TiO<sub>2</sub> could form a hydrophilic film on the membrane surface, and thus the gel layer was prevented from forming or easy to wash off after its deposition. Therefore, the anti-fouling ability of hybrid membrane was greatly

**Table 2** Properties of the membranes

samples	viscosity/(Pa·s)	maximum loading/N	elongation at break/%	porosity/%	roughness /nm
PVDF	19.5	13.0	24.1	63.3	102.1
PVDF/TiO <sub>2</sub> -5%	21.4	12.5	32.4	67.8	66.0
PVDF/TiO <sub>2</sub> -10%	29.1	11.0	41.2	74.1	45.0
PVDF/TiO <sub>2</sub> -12%	34.3	11.5	36.3	73.9	67.1



**Fig. 3** Pore size distribution for different membranes. (a) PVDF; (b) PVDF/TiO<sub>2</sub>-5%; (c) PVDF/TiO<sub>2</sub>-10%; (d) PVDF/TiO<sub>2</sub>-12%

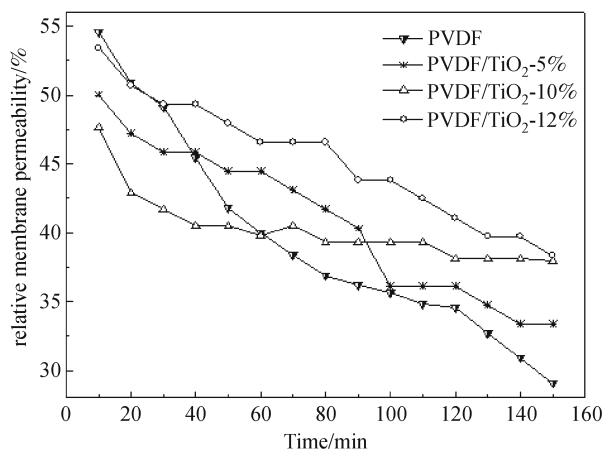


**Fig. 4** Variation of permeate flux of PVDF membranes at different titanium dioxide loadings as a function of operating time

enhanced. Besides, the flux decline ratio (the ratio of flux decline to the initial flux value) of the PVDF/TiO<sub>2</sub>-10% hybrid membrane was only 22.5%, while the ratio of the PVDF membrane was 46.7%, confirming that the surface

modification can effectively improve the hydrophilicity. The good anti-fouling ability of the hybrid membranes can be ascribed to the surface smoothness and the addition of nano-TiO<sub>2</sub> [27]. The flux of both membranes declined with the operating time due to membrane fouling. However, for the modified membranes, flux was remarkably higher than that of the unmodified membrane. These results clearly demonstrated that the surface modification substantially reduced membrane fouling.

TiO<sub>2</sub> nanoparticles played an important role in the pure water permeability and anti-fouling performance of PVDF membranes. To verify this fact and to assess the hydrophilicity of the membrane, contact angle was measured and the results are presented in Table 1. The contact angles for each membrane were tested for 9 times, and the SD was all around 1.6. As smaller contact angle indicates better hydrophilicity [28], it could be seen that the membrane hydrophilicity was improved by the addition of nano-TiO<sub>2</sub>. The pure PVDF membrane had the initial contact angle of 83°, while the initial contact angle of the hybrid membrane (10 vol.%) was 60°. It revealed that the hydrophilicity increased greatly owing to the presence of TiO<sub>2</sub> nanoparticles which contain

hydroxyl groups that can improve the hydrophilicity of the membrane surface. However, the contact angle stopped decreasing and even began increasing when TiO<sub>2</sub> concentration was over 10 vol.%. It could be interpreted that the nanoparticles aggregated when there were too many of them, reducing the amount of exposed hydroxyl groups.

### 3.2 Surface observation

#### 3.2.1 XRD

The XRD diffraction patterns of nano-sized TiO<sub>2</sub> crystal powders, PVDF/TiO<sub>2</sub>-10% and pure PVDF membrane were shown in Fig. 5. The diffraction scan of TiO<sub>2</sub> crystal powders shows characteristic crystalline peaks at  $2\theta$  of 25.3°, 37.9°, and 48.1°. In addition to the dispersion peak of amorphous PVDF membrane, the pattern of PVDF/TiO<sub>2</sub>-10% also had the three crystalline characteristic peaks of TiO<sub>2</sub>, though the corresponding peaks to TiO<sub>2</sub>/PVDF membrane is shifted left or right a little, which indicated that the nano-sized TiO<sub>2</sub> was distributed well in the membrane.

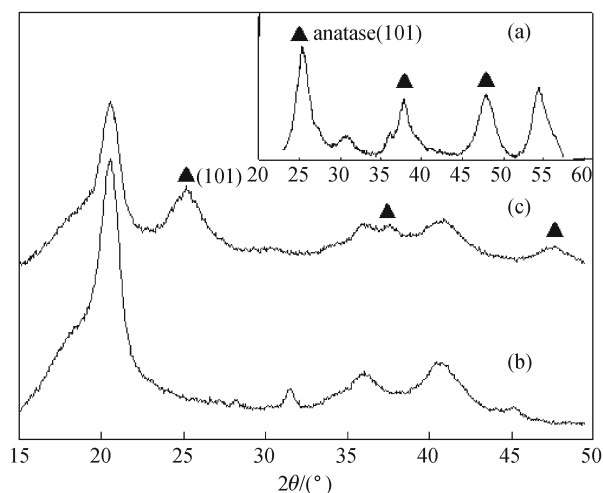


**Fig. 5** X-ray diffraction patterns of (a) TiO<sub>2</sub> nanoparticles, (b) PVDF membrane and (c) PVDF/TiO<sub>2</sub>-10% membrane

#### 3.2.2 XPS

The chemical composition for the top surfaces of both

membranes (PVDF and PVDF/TiO<sub>2</sub>-10%) was evaluated by XPS (Table 3). Since the PVDF molecule contains only hydrogen, fluorine and carbon atoms, the XPS spectrum of the hydrophilic PVDF membrane shows the representative peaks of carbon and fluorine as expected. A small amount of N (2.08 mol.%) and O (4.65 mol.%) was still detected (Figs. 6(b) and 6(c)), which might be attributed to the residue on the instrument or/and the air dust fallen on the surface of the membrane tested. After the filtration of BSA, the contents of oxygen and nitrogen increased remarkably both in pure PVDF membrane and the hybrid one, confirming the membranes had been fouled by the protein, while the increment of N and O from the hybrid membrane was much smaller than that from the pure PVDF membrane, which indicated that the anti-fouling performance of the hybrid membrane was greatly improved. Besides, the existence of Ti in the hybrid membranes was also confirmed, although the detected content of Ti was not very high.

#### 3.2.3 SEM

To study the effect of TiO<sub>2</sub> nanoparticles on the microstructure of the membranes, typical surface and cross-section SEM photographs of PVDF and PVDF/TiO<sub>2</sub>-10% membranes were obtained as illustrated in Fig. 7. From Figs. 7(a) and 7(b), it could be observed that the surface morphology of modified PVDF membranes was smoother (which could be further verified by the images of AFM in Fig. 8). And there were TiO<sub>2</sub> nanoparticles wrapped by polymers or aggregates of TiO<sub>2</sub> nanoparticles attached or embedded on the surface of PVDF/TiO<sub>2</sub> hybrid membrane, which showed that the modified nano-TiO<sub>2</sub> particles did not aggregate like the commercial ones [24] and could disperse evenly in the membrane.

From the cross-section images of these membranes shown in Figs. 7(c) and 7(d), it could be clearly observed that the topical asymmetric structure of the hybrid membrane becomes faint, the thickness of skinlayer increased and the structure of sublayer underwent a transition from finger-like to sponge-like structure. This phenomenon indicated that the drastic increase in casting solution viscosity (Table 2) by the addition of TiO<sub>2</sub> sol and the interaction between TiO<sub>2</sub> and polymers could restrict the motion of nanoparticles. Therefore, the nanoparticles were adsorbed or embedded in the skinlayer. The increase in the viscosity of the casting solution slowed down the

**Table 3** Surface element contents for different membranes

samples	C/%	O/%	N/%	F/%	Ti/%
PVDF	61.52	4.65	2.08	31.75	0
PVDF(after filtration)	64.93	22.82	9.65	2.60	0
PVDF/TiO <sub>2</sub> -10%	59.64	5.17	1.71	25.19	8.29
PVDF/TiO <sub>2</sub> -10%(after filtration)	60.73	9.17	3.68	20.34	6.08

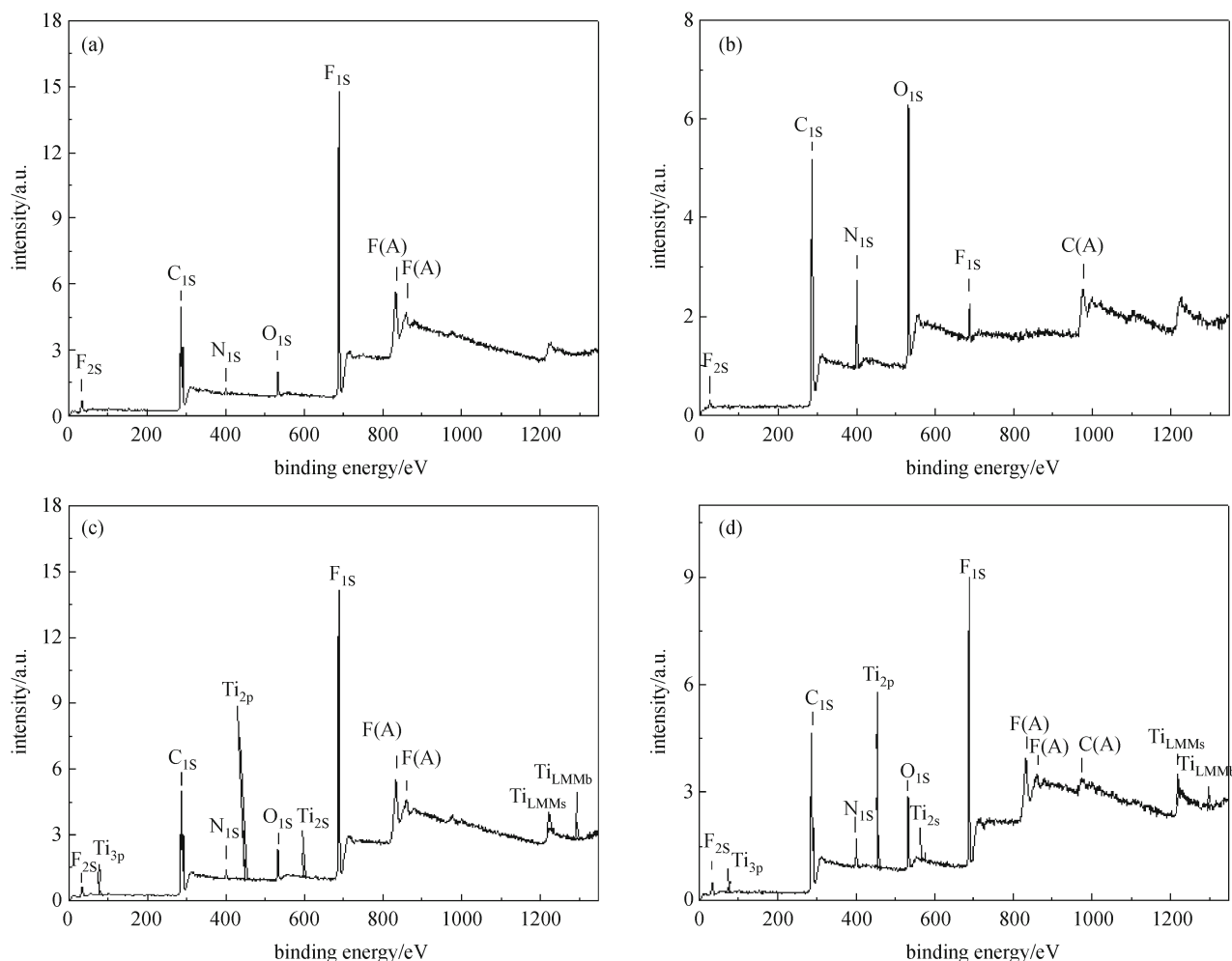


**Fig. 6** XPS spectra for different membranes before and after the filtration of BSA. (a) PVDF, before filtration; (b) PVDF, after filtration; (c) PVDF/TiO<sub>2</sub>-10%, before filtration; (d) PVDF/TiO<sub>2</sub>-10%, after filtration

exchange rate of solvent (DMAc/NMP)/nonsolvent (ethanol/water) and resulted in a delayed demixing process with macrovoids suppression.

The differences between the PVDF membrane and the hybrid membrane from the SEM morphologies reflected the effect of TiO<sub>2</sub> nanoparticles on their microstructures. The addition of TiO<sub>2</sub> nanoparticles could induce the establishment of higher crosslinking density in the inorganic-organic networks in the hybrid membranes.

### 3.2.4 AFM

Figure 8 shows the AFM images of the membrane surface over a scan area of 5  $\mu\text{m} \times 5 \mu\text{m}$ . Comparing these images, the surface seems to become rougher with an increase of TiO<sub>2</sub> sol loading. The membrane surface is rough on a nanometer scale. The RMS roughness, R<sub>q</sub>, obtained from the AFM image analysis is shown in Table 2. The average roughness of the PVDF membrane was much

higher than that of the modified ones, especially the PVDF/TiO<sub>2</sub>-10%.

This phenomenon indicates that the embedded TiO<sub>2</sub> nanoparticles fill and level up the accidented membrane surfaces in the phase inversion process, and make it smoother. Usually, a rough membrane is liable to absorbing impurities in water. Therefore, the PVDF/TiO<sub>2</sub> composite membrane with smoother surfaces may have greater antifouling capability.

### 3.2.5 FT-IR

Figure 9 shows the FT-IR spectra of the membranes. Usually, the PVDF is in a semi crystalline phases ( $\alpha$  and  $\beta$ ) and an amorphous phase. Peaks at 763 and 1179  $\text{cm}^{-1}$  were attributed to the phase vibration of  $\alpha$  and  $\beta$  crystalline, respectively. The absorption peaks at 880 and 841  $\text{cm}^{-1}$  should be attributed to the amorphous phase, and the peak at 1403  $\text{cm}^{-1}$  was due to the deformation vibration of  $-\text{CF}_2$ .

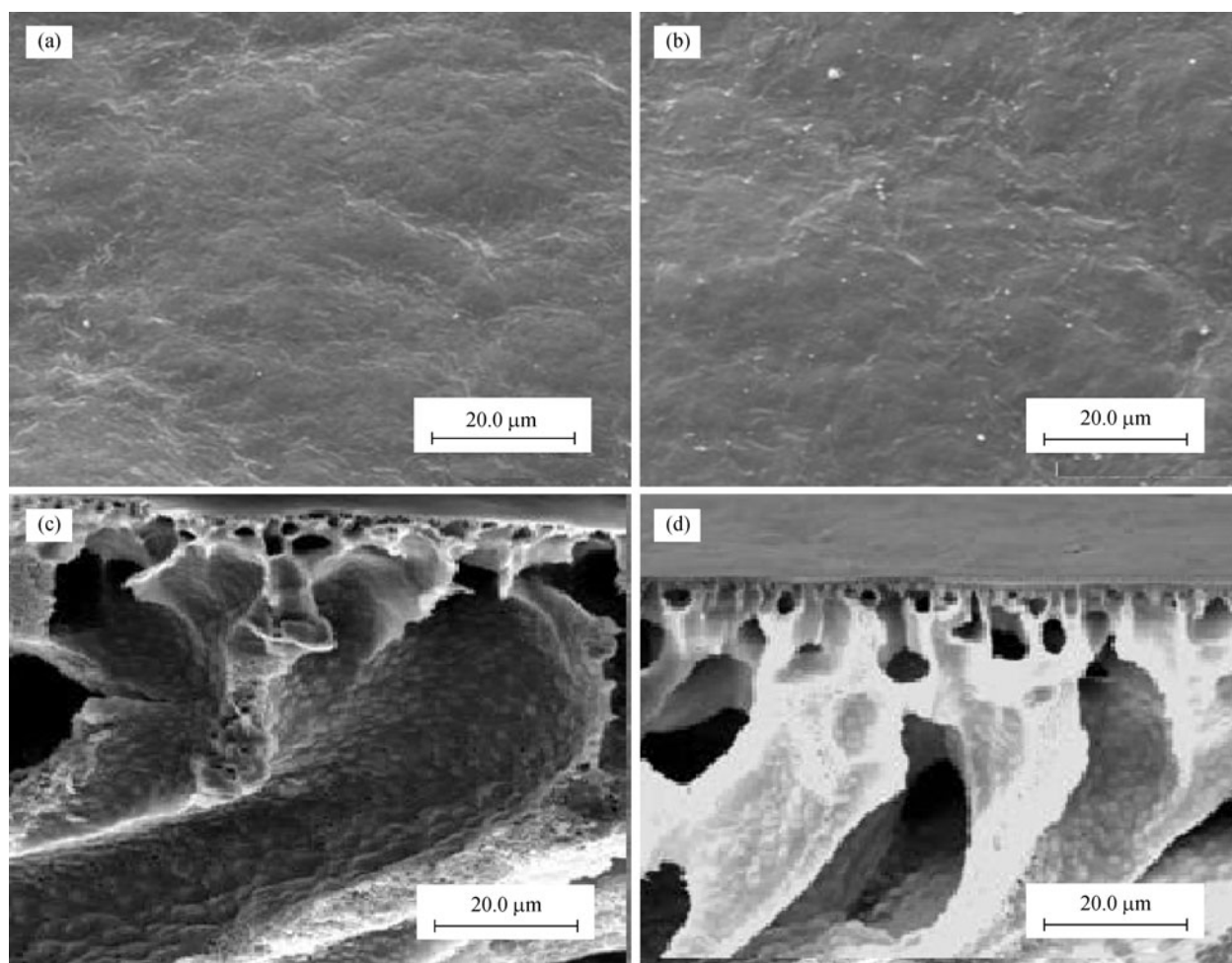


**Fig. 7** SEM micrographs of pure PVDF and TiO<sub>2</sub>-incorporated hybrid membranes. (a) Surface view of PVDF membrane; (b) surface view of PVDF/TiO<sub>2</sub>-10% membrane; (c) cross-sectional view of PVDF membrane; (d) cross-sectional view of PVDF/TiO<sub>2</sub>-10% membrane

Compared with pure PVDF membranes, a new absorption band around  $609\text{ cm}^{-1}$  could be found in the FT-IR spectra of PVDF/TiO<sub>2</sub>-X (X = 5%, 10%, 12%) membranes, which could be ascribed to the symmetric deformation vibration of Ti–O–Ti group. It indicated that the TiO<sub>2</sub> were embedded and dispersed within the hybrid membranes. Besides, the absorption peaks appearing at the interval of  $3300\text{--}3400\text{ cm}^{-1}$  were assigned to the stretching vibration of –OH groups, which also indicated the presence of TiO<sub>2</sub> in the hybrid membranes. The absorption peaks at around  $1500\text{ cm}^{-1}$  could be assigned to the vibration of the Ti–O bond [29], the intensity of which became stronger with the increase in TiO<sub>2</sub> content. It could also be observed that with the addition of nano-TiO<sub>2</sub>, a peak appears due to the vibration of the PVDF  $\beta$  phase, which further proved that the stress was the main reason for the change in PVDF crystal formation [30]. Therefore, the FT-IR spectra clearly demonstrated that TiO<sub>2</sub> was successfully incorporated into the PVDF membrane.

### 3.3 Mechanical strength

The breaking strength and elongation ratio results are listed in Table 2. The maximum loading and the elongation at break for each kind of membrane were tested for 5 times, respectively, and the SD was all under 0.5%. It is evident that the mechanical strength of membrane was enhanced with the increase of the filler concentration. At 10 vol.% filler concentration, the elongation ratio reached a peak, which was as high as 41.2%. Considering the initial value (24.1%), it was improved by 71.0%. That is, the toughness of the hybrid membrane was greatly enhanced. Compared with the elongation ratio, the variation of breaking strength was negligible. The phenomena could be interpreted by the uniform dispersion of the TiO<sub>2</sub> nanoparticles in the membrane. The TiO<sub>2</sub> nanoparticles entwined around the PVDF molecular chain and formed a network structure, which dispersed the pores more evenly. Meanwhile, the space resistance effect from the large PVDF molecular

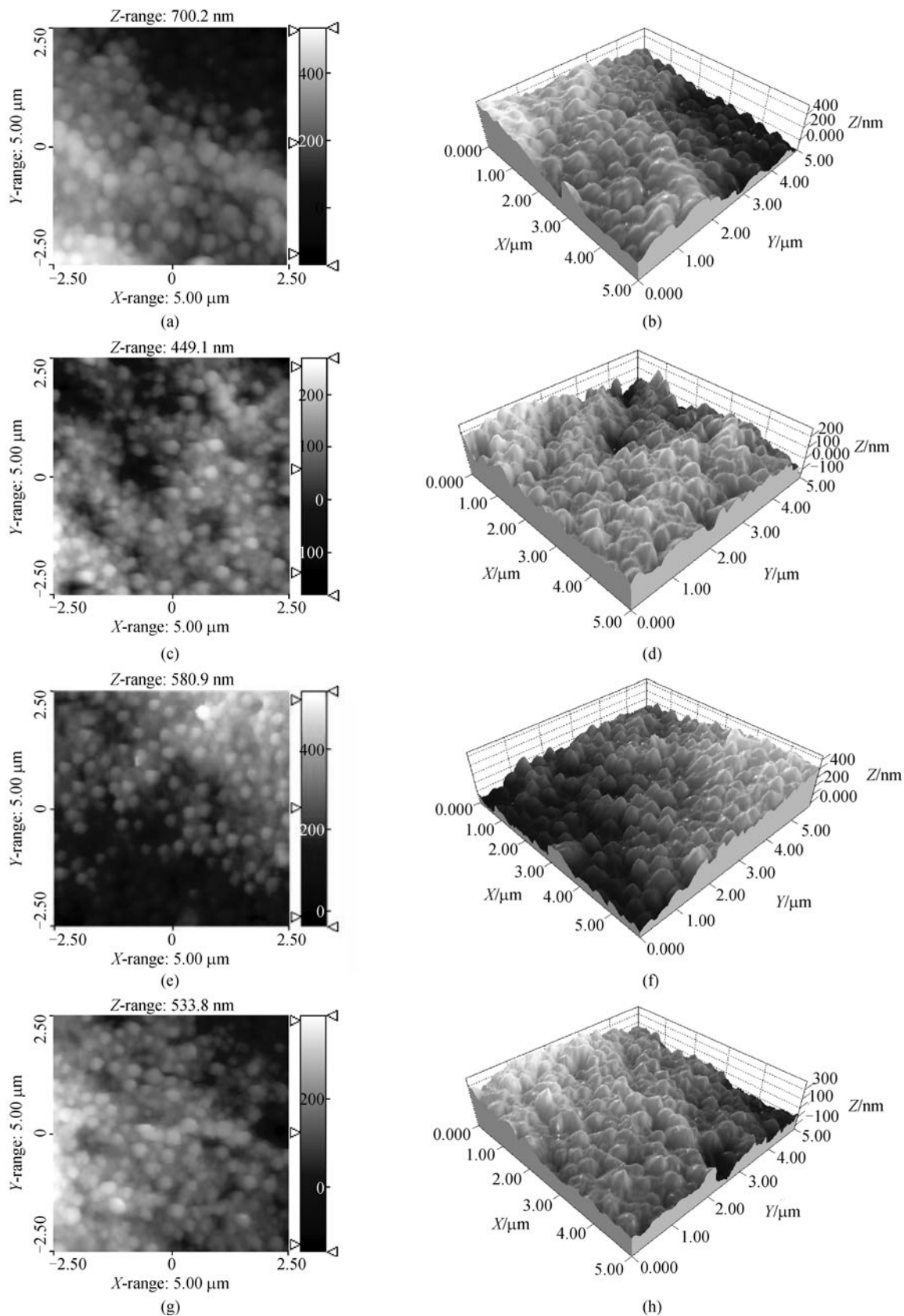


**Fig. 8** Three-dimensional AFM images of the PVDF and PVDF/TiO<sub>2</sub> hybrid membrane surfaces. (a) and (b) PVDF; (c) and (d) PVDF/TiO<sub>2</sub>-5%; (e) and (f) PVDF/TiO<sub>2</sub>-10%; (g) and (h) PVDF/TiO<sub>2</sub>-12%

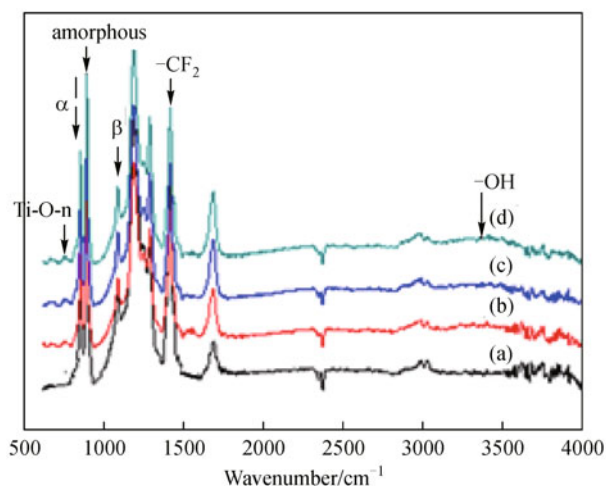


**Fig. 9** FTIR spectra of pure PVDF and TiO<sub>2</sub>-incorporated hybrid membranes. (a) PVDF; (b) PVDF/TiO<sub>2</sub>-5%; (c) PVDF/TiO<sub>2</sub>-10%; (d) PVDF/TiO<sub>2</sub>-12%

chain could also prevent the nanoparticles from aggregating, thus the mechanical strength of membranes was increased evidently. However, an excessive TiO<sub>2</sub> sol amount could cause the irreversible aggregation of nanoparticles and the formation of defects, which could correspondingly weaken mechanical stability of the hybrid membranes and made them vulnerable (with the brittle fracture).

## 4 Conclusions

Hybrid membranes were prepared by adding the nano-TiO<sub>2</sub> into the PVDF casting solution. Results showed that the nano-TiO<sub>2</sub> developed in this study could affect the properties of the membranes dramatically. Based on this study, the following conclusions could be drawn.

1) Membranes with the best properties (e.g., the highest pure water flux, the best BSA rejection, the smallest contact angle, etc.) were obtained by adding 10 vol.% nano-TiO<sub>2</sub> to the PVDF casting solution. The pure water flux attained as high as 257 L·m<sup>-2</sup>·h<sup>-1</sup> (65.9% higher than that of the pure PVDF membrane), the rejection was up to 74.1% (21.8% higher than that of the pure PVDF membrane) and the porosity was 15.0% higher than the pure PVDF membrane.

2) Contact angle of the hybrid membranes was decreased, indicating the enhanced hydrophilicity for the hybrid membranes.

3) Analysis from XPS confirmed that the antifouling characteristics of the modified membranes were greatly enhanced, as the amounts of elements from the modified PVDF membranes were much less than those from the pure PVDF membranes after the filtration of BSA solution. It was also confirmed by the fact that the decreasing rate of permeate flux of the hybrid membrane was obviously

lower than that of the pure PVDF membrane, and the flux recovery after water cleaning was also much higher.

4) Surface analysis (including SEM, AFM, pore size distribution, FT-IR and XRD) confirmed that surface of the hybrid membranes was smooth and the TiO<sub>2</sub> nanoparticles were dispersed uniformly, resulting in a better compatibility between the polymer chains and TiO<sub>2</sub> nanoparticles. Moreover, the amount of hydroxyl groups in the membrane surface was increased while the pore size distribution was narrowed.

**Acknowledgements** This research was supported by the State Key Laboratory Foundation of Ministry of Science and Technology of China (Nos. PCRRY09004 and PCRRF08009), the Key Special Program on Science and Technology for Water Pollution Control and Governance (No. 2012ZX07403001), International Science & Technology Cooperation Program of China (No. S2011ZR0434) and Study on Campus Drinking Water Project of Shuitian, Tongji University, China (No. STSJ2011100).

## References

1. Wu L, Sun J, Wang Q. Poly(vinylidene fluoride)/polyethersulfone blend membranes: effects of solvent sort, polyethersulfone and polyvinylpyrrolidone concentration on their properties and morphology. *Journal of Membrane Science*, 2006, 285(1–2): 290–298
2. Wu L S, Sun J F, Wang Q R. Study progress of poly(vinylidene fluoride) membrane. *Chinese Journal of Membrane Science and Technology*, 2004, 24(5): 63–68 (in Chinese)
3. Du J R, Peldszus S, Huck P M, Feng X. Modification of poly(vinylidene fluoride) ultrafiltration membranes with poly(vinyl alcohol) for fouling control in drinking water treatment. *Water Research*, 2009, 43(18): 4559–4568
4. Du Q Y. Study on the preparation and application of PVDF hollow fiber membrane. *Chinese Journal of Membrane Science and Technology*, 2003, 23(4): 80–85 (in Chinese)
5. Zuo D Y, Xu Y Y, Zou H T. Research on two-steps formation mechanism of PVDF membrane by immersion precipitation. *Chinese Journal of Membrane Science and Technology*, 2009, 29(1): 29–35 (in Chinese)
6. Cao X, Ma J, Shi X, Ren Z. Effect of TiO<sub>2</sub> nanoparticle size on the performance of PVDF membrane. *Applied Surface Science*, 2006, 253(4): 2003–2010
7. Zhang Y Q, Zhang H L, Qu Y. Effects of addition of nano-SiO<sub>2</sub> particles on polyvinylidene fluoride (PVDF) based membrane performance. *Chinese Journal of Membrane Science and Technology*, 2007, 27(6): 47–51 (in Chinese)
8. Zhao Y H, Qian Y L, Zhu B K, Xu Y Y. Modification of porous poly(vinylidene fluoride) membrane using amphiphilic polymers with different structures in phase inversion process. *Journal of Membrane Science*, 2008, 310(1–2): 567–576
9. Yu H Y, He X C, Liu L Q, Gu J S, Wei X W. Surface modification of polypropylene microporous membrane to improve its antifouling characteristics in an SMBR: N<sub>2</sub> plasma treatment. *Water Research*, 2007, 41(20): 4703–4709
10. Di Vona M L, Marani D, D'Epifanio A, Traversa E, Trombetta M, Licocchia S. A covalent organic/inorganic hybrid proton exchange

- polymeric membrane: synthesis and characterization. *Polymer*, 2005, 46(6): 1754–1758
11. Xue S, Yin G. Proton exchange membranes based on poly(vinylidene fluoride) and sulfonated poly(ether ether ketone). *Polymer*, 2006, 47(14): 5044–5049
  12. Lu Y, Yu S L, Chai B X. Preparation of poly(vinylidene fluoride) (PVDF) ultrafiltration membrane modified by nano-sized alumina ( $\text{Al}_2\text{O}_3$ ) and its antifouling research. *Polymer*, 2005, 46(18): 7701–7706
  13. Yu S L, Zuo X T, Bao R L, Xu X, Wang J, Xu J. Effect of  $\text{SiO}_2$  nanoparticle addition on the characteristics of a new organic–inorganic hybrid membrane. *Polymer*, 2009, 50(2): 553–559
  14. Zhao P, Fan J. Electrospun nylon 6 fibrous membrane coated with rice-like  $\text{TiO}_2$  nanoparticles by an ultrasonic-assistance method. *Journal of Membrane Science*, 2010, 355(1–2): 91–97
  15. He P, Zhao A C. Nanometer composite technology and application in polymer modification. *Polymer Bulletin*, 2001, 2(1): 74–82 (in Chinese)
  16. Khayet M, Villaluenga J P G, Valentin J L, Lepez-Manchado M A, Mengual J I, Seoane B. Filled poly(2,6-dimethyl-1,4-phenylene oxide) dense membranes by silica and silane modified silica nanoparticles: characterization and application in pervaporation. *Polymer*, 2005, 46(23): 9881–9891
  17. Bottino A, Capannelli G, Comite A. Preparation and characterization of novel porous PVDF- $\text{ZrO}_2$  composite membranes. *Desalination*, 2002, 146(1–3): 35–40
  18. Zhou H, Chen Y, Fan H, Shi H, Luo Z, Shi B. Water vapor permeability of the polyurethane/ $\text{TiO}_2$  nanohybrid membrane with temperature sensitivity. *Journal of Applied Polymer Science*, 2008, 109(5): 3002–3007
  19. Vona M L D, Ahmed Z, Bellitto S, Lenci A, Traversa E, Licocchia S. SPEEK- $\text{TiO}_2$  nanocomposite hybrid proton conductive membranes via in situ mixed sol–gel process. *Journal of Membrane Science*, 2007, 296(1–2): 156–161
  20. Yang Y, Wang P. Preparation and characterizations of a new PS/ $\text{TiO}_2$  hybrid membrane by sol–gel process. *Polymer*, 2006, 47(8): 2683–2688
  21. Zuo D Y, Xu Y Y, Zhang Z. Preparation and performance researches on PVDF microporous flat membrane with the large pore diameter. *Technology of Water Treatment*, 2008, 34(6): 8–11 (in Chinese)
  22. Fu X, Matsuyama H, Nagai H. Structure control of a symmetric poly(vinyl butyral)- $\text{TiO}_2$  composite membrane prepared by nonsolvent induced phase separation. *Journal of Applied Polymer Science*, 2008, 108(2): 713–723
  23. Amjadi M, Rowshanzamir S, Peighambaroust S J, Hosseini M G, Eikani M H. Investigation of physical properties and cell performance of Nafion/ $\text{TiO}_2$  nanocomposite membranes for high temperature PEM fuel cells. *International Journal of Hydrogen Energy*, 2010, 35(17): 9252–9260
  24. Bae T H M, Tak T M. Effect of  $\text{TiO}_2$  nanoparticles on fouling mitigation of ultrafiltration membranes for activated sludge filtration. *Journal of Membrane Science*, 2005, 249(1–2): 1–8
  25. Ju X S, Huang P, Xu N P, Shi J. Study of factors influencing pore size of zirconia ultrafiltration membrane. *Chinese Journal of Chemical Engineering*, 2000, 14(2): 103–108 (in Chinese)
  26. Yang D, Li J, Jiang Z, Lu L, Chen X. Chitosan/ $\text{TiO}_2$  nanocomposite pervaporation membranes for ethanol dehydration. *Chemical Engineering Science*, 2009, 64(13): 3130–3137
  27. Cioffi N, Torsi L, Ditaranto N, Tantillo G, Ghibelli L, Sabbatini L, Bleve-Zacheo T, D’Alessio M, Zamboni P G, Traversa E. Copper nanoparticle/polymer composites with antifungal and bacteriostatic properties. *Chemistry of Materials*, 2005, 17(21): 5255–5262
  28. Jiang H F, Ma Y X, Wang D, Gao C J. Preparation and characterization of polymer/ $\text{TiO}_2$  hybrid membrane. *Functional Materials*, 2008, 40(4): 591–594
  29. Hu Q, Marand E, Dhingra S. Poly(amide-imide)/ $\text{TiO}_2$  nanocomposite gas separation membranes: fabrication and characterization. *Journal of Membrane Science*, 1997, 135(1): 65–79
  30. Ren P, Zhang H, Zhang G F. Study on Crystal Phase in PVDF Melt Spun Fibre. *Journal of Tianjin Polytechnic University*, 2003, 22(4): 8–13 (in Chinese)